pubs.acs.org/IC

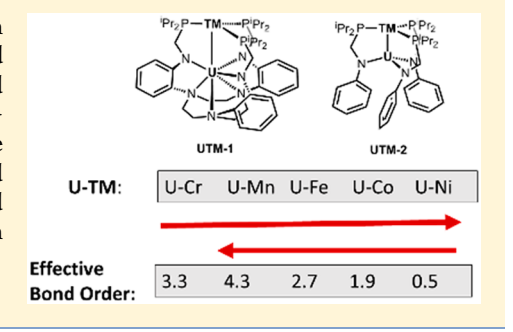
# Multiple Bonds in Uranium—Transition Metal Complexes

Prachi Sharma, †,‡® Dale R. Pahls,†,‡ Bianca L. Ramirez,†® Connie C. Lu,†® and Laura Gagliardi\*,†,‡®

Department of Chemistry and \*Minnesota Supercomputing Institute & Chemical Theory Center, University of Minnesota, Minneapolis, Minnesota 55455-0431, United States

Supporting Information

ABSTRACT: Novel heterobimetallic complexes featuring a uranium atom paired with a first-row transition metal have been computationally predicted and analyzed using density functional theory and multireference wave function based methods. The synthetically inspired metalloligands U{(iPr<sub>2</sub>PCH<sub>2</sub>NAr)<sub>3</sub>tacn} (1) and U(Pr<sub>2</sub>PCH<sub>2</sub>NPh)<sub>3</sub> (2) are explored in this study. We report the presence of multiple bonds between uranium and chromium, uranium and manganese, and uranium and iron. The calculations predict a 5-fold bonding between uranium and manganese in the UMn(iPr<sub>2</sub>PCH<sub>2</sub>NPh)<sub>3</sub> complex, which is unprecedented in the literature.



### 1. INTRODUCTION

Metal-metal bonding is a fundamental concept in chemistry that affects the properties of the systems of interest and is instrumental to understanding structure and reactivity, metalsurface chemistry, and metal-based catalysis. Compared to transition metals, the nature of metal-metal bonds involving f-block metals, especially the actinide series, has been less explored. The 5f orbitals of the actinides, such as uranium, have suitable spatial extension to participate in bonding, which makes the d-f heterobimetallic bond an interesting target to improve our understanding of the interplay of the d and f orbitals.

A review of both theoretical and experimental data in the literature shows that very few examples have been reported for bonding between an actinide, such as uranium, and a transition metal to date. The first attempt to synthesize a uraniumtransition metal (U-TM) compound was made by Stone in 1971. He reported the synthesis of a uranium-manganese complex with carbonyl ligands; however, the complex, being highly air sensitive, decomposed before it could be analyzed. In 1987, Sternal and Marks<sup>4</sup> reported the successful synthesis of uranium-ruthenium and uranium-iron complexes, although the X-ray diffraction was not reported for these complexes. Although U-TM complexes are promising, the research in the field had been dormant for more than a decade. Later in 2000, Ephritikhine and co-workers<sup>5</sup> reported the successful synthesis and characterization of urana[1]ferrocenophane compounds with Fe-U-Fe bonds, where the average U-Fe bond length is 3.14 Å, which is shorter than the covalent U-Fe distance of 3.28 Å.6 Since then, several bimetallic U-TM complexes have been reported in the literature, including experimental and predominantly theoretical studies.8

The bonding interactions in these previously reported U-TM compounds are predominantly dative; 7d,f,h,j,m,o however, minor  $\sigma$  and  $\pi$  contributions were also predicted in some complexes by computational calculations.

Bimetallic complexes generally contain numerous low-lying states, and therefore, it is important to use a multireference method to accurately predict the nature of chemical bonding.<sup>14</sup> Multireference methods, such as complete active-space selfconsistent field method (CASSCF), have been employed to explore the bonding of f-block metals, particularly in uranium chemistry. 8a,c,e,10 Multireference calculations have predicted the existence of high bond orders in the uranium-uranium bond of U2. 10d,f Furthermore, multiple computational studies have been used to explore uranium-ligand bonding, 10a,b,11 and uranium-transition metal chemistry.

In this article, we explore the chemical bonding between a first-row transition metal and a uranium atom in UTM-[(<sup>i</sup>Pr<sub>2</sub>PCH<sub>2</sub>NAr)<sub>3</sub>tacn] (UTM-1) and UTM(<sup>i</sup>Pr<sub>2</sub>PCH<sub>2</sub>NPh)<sub>3</sub> (UTM-2) species, where TM = Cr, Mn, Fe, Co, Ni. UTM-1 and UTM-2 are comprised of nonadentate (¹Pr<sub>2</sub>PCH<sub>2</sub>NHAr)<sub>3</sub>tacn and bidendate <sup>i</sup>Pr<sub>2</sub>PCH<sub>2</sub>NHPh ligands, respectively; both contain hard amido and soft phosphine groups. We focus on first-row transition metals because the 5f-3d interactions are less explored compared to f-block and second-row transition metals and, because of the unique electronic structures and greater spin-flexibility

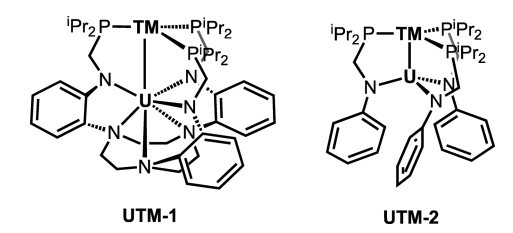


Figure 1. Schematic representation of (left) UTM[(iPr2PCH2-NAr)<sub>3</sub>tacn (UTM-1) and (right) UTM(<sup>i</sup>Pr<sub>2</sub>PCH<sub>2</sub>NPh)<sub>3</sub> (UTM-2), where  $TM = \{Cr, Mn, Fe, Co, Ni\}.$ 

Received: April 30, 2019 Published: July 22, 2019

Table 1. Geometrical Parameters, Including Bond Lengths ( $\mathring{A}$ ) and Angles (deg) for UTM-1 Obtained from DFT Calculations<sup>a</sup>

UTM		U	Cr			UMn			UFe			UCo		U	Ni
spin $(2S + 1)$	2	4	6	8	1	3	5	2	4	6	1	3	5	2	4
Cal. $S^2$	0.75	3.75	8.75	15.75	0.00	2.00	6.00	0.75	3.75	8.75	0.02	2.00	6.00	0.77	3.75
U-TM	1.99	2.07	2.28	3.00	1.94	2.03	2.17	2.02	2.20	2.75	2.25	2.26	2.63	2.68	2.72
avg TM-P	2.40	2.39	2.38	2.37	2.35	2.32	2.34	2.28	2.27	2.24	2.22	2.22	2.22	2.20	2.21
avg U-N <sub>tacn</sub>	2.80	2.78	2.78	2.73	2.79	2.80	2.79	2.80	2.81	2.75	2.80	2.80	2.78	2.76	2.76
avg $U-N_{amide}$	2.41	2.45	2.44	2.41	2.40	2.44	2.45	2.42	2.43	2.41	2.40	2.40	2.41	2.38	2.40
$E^{\mathrm{DFT}}$ (kcal/mol)	0.0	11.6	27.6	41.6	0.0	13.3	37.1	0.0	20.1	47.2	7.5	0.0	28.8	10.2	0.0
$FSR^b$	0.68	0.71	0.78	1.03	0.67	0.70	0.84	0.71	0.77	0.96	0.80	0.80	0.94	0.96	0.97

<sup>&</sup>lt;sup>a</sup>Bond lengths in angstroms (Å). The most stable spin states are shown in bold text. <sup>b</sup>FSR: Formal shortness ratio; defined as the ratio between the calculated bond length and the sum of covalent radii of the two metals.

Table 2. Geometrical Parameters, Including Bond Lengths (Å) and Angles (deg) for UTM-2 Obtained from DFT Calculations<sup>a</sup>

UTM		Ü	JCr			UMn			UFe			UCo		U	Ni
spin $(2S + 1)$	2	4	6	8	1	3	5	2	4	6	1	3	5	2	4
Cal. S <sup>2</sup>	0.75	3.75	8.75	15.75	1.00	2.00	6.00	0.75	3.75	8.75	0.03	2.00	6.00	0.79	3.75
U-TM	1.99	2.07	2.29	2.75	1.94	2.03	2.20	2.02	2.21	2.62	2.23	2.25	2.47	2.64	2.62
avg TM-P	2.39	2.41	2.39	2.36	2.35	2.33	2.35	2.30	2.28	2.27	2.24	2.23	2.24	2.21	2.24
avg U-N <sub>amide</sub>	2.38	2.38	2.37	2.41	2.36	2.37	2.37	2.35	2.36	2.32	2.33	2.34	2.34	2.30	2.33
$E^{\mathrm{DFT}}(\mathrm{kcal/mol})$	0.0	13.0	26.9	41.9	0.0	19.6	45.3	0.0	19.6	45.3	6.8	0.0	28.0	4.7	0.0
$E^{\text{CASSCF}}(\text{kcal/mol})$	0.0	5.2	-0.4	14.2	0.0	15.2	21.4	0.0	6.9	38.8	21.3	0.0	57.7	10.7	0.0
E <sup>CASPT2</sup> (kcal/mol)	0.0	22.7	29.1	47.6	0.0	38.5	73.1	0.0	26.5	83.8	14.4	0.0	64.3	22.3	0.0
FSR <sup>b</sup>	0.68	0.71	0.78	0.94	0.67	0.70	0.76	0.70	0.77	0.91	0.80	0.80	0.88	0.94	0.94

<sup>&</sup>quot;Bond lengths in angstroms (Å). The most stable spin states are shown in bold text. Relative energies with respect to the most stable spin-state are calculated at DFT, CASSCF, and CASPT2 levels of theory. "FSR: Formal shortness ratio; defined as the ratio between the calculated bond length and the sum of covalent radii of the two metals.

Table 3. Mayer Bond Order (BO) Calculated at DFT Level for Ground Spin State for UTM-1 and UTM-2 Complexes

	UCr	UMn	UFe	UCo	UNi
Mayer BO UTM-1	3.3	3.6	2.8	1.5	0.5
Mayer BO UTM-2	3.3	3.6	2.9	1.5	0.7

of first-row transition metals, these interactions might have unique features. The structures of the potential U-TM complexes are shown in Figure 1. The complexes hypothesized

here are inspired by previous work by Ramirez et al., <sup>12</sup> in which the same ligands were employed to make 4f–3d Lu–Ni bimetallic species. In this study, we employ density functional theory (DFT) and multireference methods to predict the stability and nature of the bonding in these novel complexes.

# 2. COMPUTATIONS

The structures of UTM-1 and UTM-2 (TM = Cr, Mn, Fe, Co, and Ni) were optimized with the PBE<sup>13</sup> functional with D3 dispersion

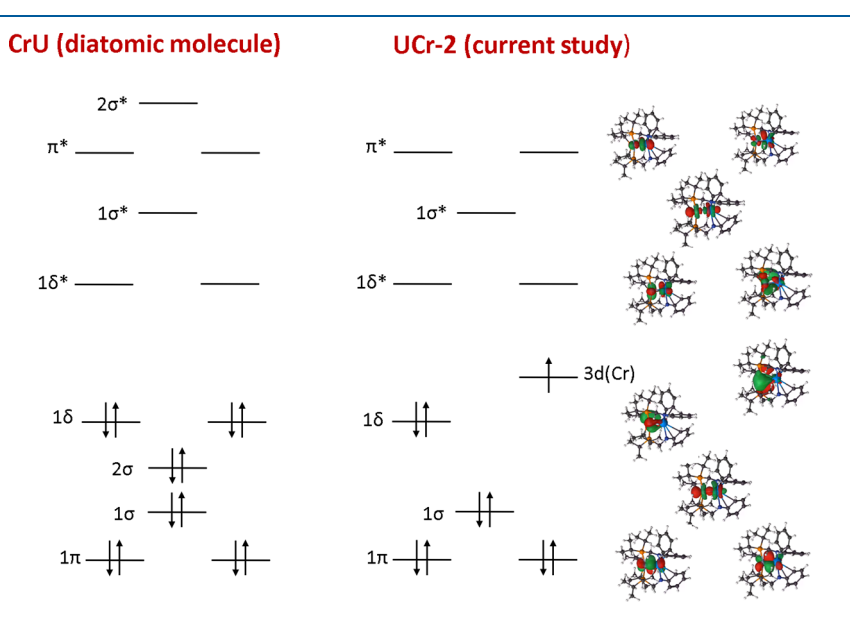


Figure 2. Comparison between the MO diagrams of CrU diatomic molecule reported in ref 8e and UCr-2 complexes.

Table 4. Detailed CASSCF Orbital Analysis of UTM-2 Species<sup>a</sup>

UCr2 σ 48.5 51.5 1.78 3.3 80   (48.3); 3d-92.4) (5f.88.2; 7p;4.1) 1.91 4.8 1.91 4.8 1.91 4.8 1.91 4.8 1.91 4.8 1.91 4.8 1.91 4.8 1.91 4.8 1.91 4.8 1.91 4.8 1.8 4.8 1.8 4.8 1.8 4.8 1.8 4.8 1.8 4.8 1.8 4.8 1.8 4.3 6.9 1.8 1.8 4.3 6.9 1.8 4.3 6.9 1.8 4.3 6.9 1.8 4.3 6.9 1.8 4.3 6.9 1.8 4.3 6.9 6.9 1.7 4.3 1.8 4.3 6.9 6.9 1.7 1.9 4.3 1.9	complex	orbital	%TM	%U	total electrons	EBO	percent of main configuration (%)
Mathematical Ma	UCr-2	σ	48.5	51.5	1.78	3.3	80
$ \begin{array}{c ccccccccccccccccccccccccccccccccccc$			(4s:3.9; 3d:92.4)	(5f:88.2; 7p:4.1)			
March   Section   Secti		$\pi$	63.2	36.8	1.91		
$ \begin{array}{c ccccccccccccccccccccccccccccccccccc$			(3d:99.9)	(6d: 60.9; 5f: 39.1)			
UMn-2 δ 52.2 47.8 1.67   UMn-2 σ (34.96), 4s; 2.9) (56.99)   UMn-2 σ (34.97.2; 4p; 2.8) (5f. 96.0; 6d.4.0) 1.85 4.3 69   μ (34.97.2; 4p; 2.8) (5f. 96.0; 6d.4.0) 1.91		$\pi$	66.5	33.6	1.91		
$ \begin{array}{c ccccccccccccccccccccccccccccccccccc$			(3d: 99.9)	(6d: 65.5; 5f:34.5)			
$ \begin{array}{c ccccccccccccccccccccccccccccccccccc$		$\delta$	52.2	47.8	1.67		
$ \begin{array}{c ccccccccccccccccccccccccccccccccccc$			(3d: 96.9; 4s: 2.9)	(5f: 99.9)			
$ \begin{array}{c ccccccccccccccccccccccccccccccccccc$	UMn-2	$\sigma$	60.2	39.8	1.85	4.3	69
$ \begin{array}{c ccccccccccccccccccccccccccccccccccc$			(3d:97.2; 4p: 2.8)	(5f: 96.0; 6d:4.0)			
$ \begin{array}{c ccccccccccccccccccccccccccccccccccc$		$\pi$	69.7(3d: 99.9)	30.3(6d; 60.4; 5f: 34.9)	1.91		
$ \begin{array}{c ccccccccccccccccccccccccccccccccccc$		$\pi$	68.7	31.3	1.91		
$ \begin{array}{c ccccccccccccccccccccccccccccccccccc$			(3d: 99.9)	(6d:57.8; 5f:38.1)			
$ \begin{array}{c ccccccccccccccccccccccccccccccccccc$		$\delta$	75.7	24.3	1.81		
$ \begin{array}{c} \text{UFe-2} \\ \text{UFe-2} \\ \text{VFe-2} \\ \text{VP-2} \\ \text{VFe-2} \\ \text{VFe-2} \\ \text{VFe-2} \\ \text{VFe-2} \\ \text{VFe-2} \\ \text{VP-2} \\ \text{VFe-2} \\ VFe$			(3d: 96.3; 4p: 3.7)	(5f:95.8; 6d:4.2)			
$ \begin{array}{c ccccccccccccccccccccccccccccccccccc$		$\delta$	71.3	28.7	1.77		
$ \begin{array}{c} \pi \\ \pi \\ 77.7 \\ 3d; 98.3; \ 4p:1.7) \\ (5d: 59.2; \ 5f: 34.5) \\ \pi \\ 75.4 \\ (3d: 99.9) \\ (6d: 58.9; \ 5f: 34.9) \\ (5d: 58.9; \ 5f: 34.9) \\ (3d: 99.9) \\ (5d: 58.9; \ 5f: 34.9) \\ (3d: 99.9) \\ (3d: $			(3d:96.3; 4s:3.7)	(6d:4.8; 5f:95.1)			
$\begin{array}{cccccccccccccccccccccccccccccccccccc$	UFe-2	$\sigma$	65.3	34.7	1.82	2.7	78
$ \begin{array}{c} R \\ R $			(3d: 99.9)	(6d:9.2; 5f:90.7)			
$\begin{array}{cccccccccccccccccccccccccccccccccccc$		$\pi$	77.7	22.3	1.91		
$ \begin{array}{c} 3d(Fe)-5f/6d(U) & 95.7 & 4.3 & 1.92 \\ 3d(Fe)-5f/6d(U) & 95.7 & 4.3 & 1.92 \\ 3d(Fe)-5f/6d(U) & 97.2 & 2.8 & 1.93 \\ 3d(Fe)-5f/6d(U) & 97.2 & 10.3 & 1.93 \\ 3d(Fe)-5f/6d(U) & 88.2 & 10.3 & 1.93 \\ 3d(Fe)-5f/6d(U) & 88.2 & 10.3 & 1.93 \\ 3d(Fe)-5f/6d(U) & 88.3 & 10.0 & 1.93 \\ 3d(Fe)-5f/6d(U) & 91.8(3d:95.4; 4p:3.7) & 8.2(7s:20.7; 6d:79.3) & 1.94 \\ 3d(Co)-5f/6d(U) & 95.9 & 4.2 & 1.94 \\ 3d(Co)-5f/6d(U) & 95.9 & 4.2 & 1.94 \\ 3d(Fe)-5f/6d(U) & 95$			(3d:98.3; 4p:1.7)	(6d:59.2; 5f:34.5)			
$ \begin{array}{cccccccccccccccccccccccccccccccccccc$		$\pi$	75.4	24.6	1.91		
$ \begin{array}{c} & 3d(Fe)-5f/6d(U) \\ 3d(Fe)-5f/6d(U) \\ & 97.2 \\ (3d:95.9; 4p:3.9) \\ & (6d:46.4; 5f:53.5) \\ \\ UCo-2 \\ & 3d/4p(Co)-6d(U) \\ & 88.2 \\ & (3d:98.3; 4p:1.6) \\ & (6d:99.9) \\ \\ & 3d/4p(Co)-5f/6d(U) \\ & 88.3 \\ & (3d:97.9; 4p:2.0) \\ & (6d:85.0; 5f:1.5) \\ & 3d(Co)-5f/6d(U) \\ & 91.8(3d:95.4; 4p:3.7) \\ & 3d(Co)-5f/6d(U) \\ & 95.9 \\ & 4.2 \\ & 1.94 \\ \\ & (3d:97.7; 4p:2.3) \\ & (7s:33.3; 6d:66.7) \\ \\ UNi-2 \\ & 3d/4s/4p(Ni)-5f/6d(U) \\ & 34.5 \\ & (3d:31.6; 4p:37.1; 4s:28.4) \\ & (7s:41.8; 6d:38.8; 5f:13.5) \\ & 3d/4s(Ni)-7s/6d(U) \\ & 88.6 \\ & 11.4 \\ & 1.95 \\ \\ \end{array} $			(3d: 99.9)	(6d:58.9; 5f:34.9)			
$ \begin{array}{cccccccccccccccccccccccccccccccccccc$		3d(Fe)-5f/6d(U)	95.7	4.3	1.92		
$ \begin{array}{c} UCo-2 \\ UCo-2 \\ VCo-2 $			(3d:95.8; 4p:4.1)	(6d:32.5; 5f:67.4)			
$\begin{array}{c} \text{UCo-2} \\ & 3d/4p(\text{Co}) - 6d(\text{U}) \\ & 3d/4p(\text{Co}) - 5f/6d(\text{U}) \\ & 3d/4p(\text{Co}) - 5f/6d(\text{U}) \\ & 3d(\text{So}) + 9 + 9 + 2.0 \\ & 3d(\text{Co}) - 5f/6d(\text{U}) \\ & 3d(\text{Co}) - 5f/6d(\text{U}) \\ & 3d(\text{Co}) - 5f/6d(\text{U}) \\ & 91.8(3d.95.4; \ 4p:3.7) \\ & 3d(\text{Co}) - 5f/6d(\text{U}) \\ & 95.9 \\ & 4.2 \\ & (3d.97.7; \ 4p:2.3) \\ & (7s:33.3; \ 6d:66.7) \\ \\ \text{UNi-2} \\ & 3d/4s/4p(\text{Ni}) - 5f/6d(\text{U}) \\ & 3d/4s(\text{Ni}) - 7s/6d(\text{U}) \\ & 88.6 \\ & 11.4 \\ & 1.95 \\ \end{array}$		3d(Fe)-5f/6d(U)	97.2	2.8	1.93		
$ \begin{array}{cccccccccccccccccccccccccccccccccccc$			(3d:95.9; 4p:3.9)	(6d:46.4; 5f:53.5)			
$ \begin{array}{cccccccccccccccccccccccccccccccccccc$	UCo-2	3d/4p(Co)-6d(U)	88.2	10.3	1.93	1.9	86
$ \begin{array}{cccccccccccccccccccccccccccccccccccc$			(3d:98.3; 4p:1.6)	(6d:99.9)			
$ \begin{array}{cccccccccccccccccccccccccccccccccccc$		3d/4p(Co)-5f/6d(U)	88.3	10.0	1.93		
$ \begin{array}{cccccccccccccccccccccccccccccccccccc$			(3d:97.9; 4p:2.0)	(6d:85.0; 5f:1.5)			
$\begin{array}{cccccccccccccccccccccccccccccccccccc$		3d(Co)-5f/6d(U)	91.8(3d:95.4; 4p:3.7)	8.2(7s:20.7; 6d:79.3)	1.94		
UNi-2 3d/4s/4p(Ni)-5f/6d(U) 34.5 57.7 1.01 0.5 91 (3d:31.6; 4p:37.1; 4s:28.4) (7s:41.8;6d:38.8; 5f:13.5) 3d/4s(Ni)-7s/6d(U) 88.6 11.4 1.95		3d(Co)-5f/6d(U)	95.9	4.2	1.94		
(3d:31.6; 4p:37.1; 4s:28.4) (7s:41.8;6d:38.8; 5f:13.5) 3d/4s(Ni)-7s/6d(U) 88.6 11.4 1.95			(3d:97.7; 4p:2.3)	(7s:33.3; 6d:66.7)			
3d/4s(Ni)-7s/6d(U) 88.6 11.4 1.95	UNi-2	3d/4s/4p(Ni)-5f/6d(U)	34.5	57.7	1.01	0.5	91
			(3d:31.6; 4p:37.1; 4s:28.4)	(7s:41.8;6d:38.8; 5f:13.5)			
(3d:97.4; 4s:2.6) (6d:66.7; 7s:33.3)		3d/4s(Ni)-7s/6d(U)	88.6	11.4	1.95		
			(3d:97.4; 4s:2.6)	(6d:66.7; 7s:33.3)			

<sup>&</sup>quot;For each orbital, we report the % contribution on the TM and on U and its composition in terms of atomic orbitals. Only natural MOs with an overlap percentage higher than 10% from either metal are considered as bonding MOs.

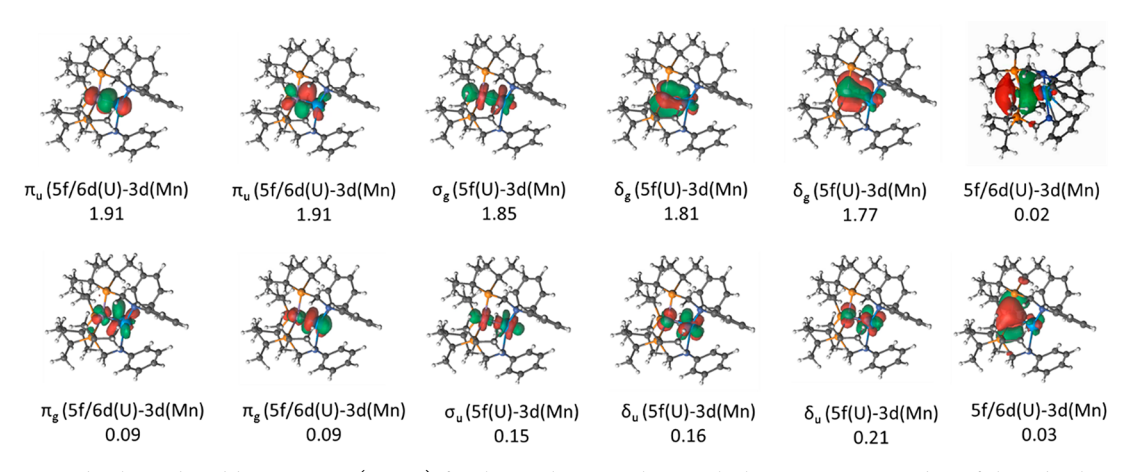


Figure 3. UMn-2 orbitals predicted by CASSCF (10, 12) for the singlet state along with the occupation number of the orbitals.

correction, 14 using the unrestricted formalism, UPBE-D3. UPBE-D3 gave satisfactory results for related bimetallic systems featuring the

same ligand.  $^{12}$  The def2-TZVP basis set $^{15}$  was used for the transition metals, N and P, while the Stuttgart/Dresden pseudopotential  $^{16}$  was

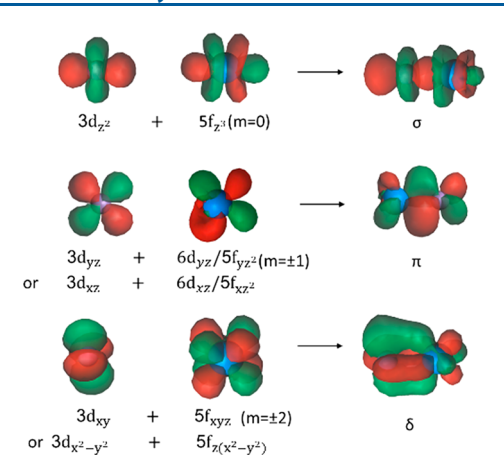


Figure 4. Combinations of the metal 3d, 5f, and 6d atomic orbitals that participate in metal—metal bonding in UMn-2 complex.

Table 5. MS-CASPT2 Excitation Energies from  $S_0$  in eV and nm for the Lowest Singlet and Triplet States and Their Electronic Configurations for UMn-2

state	E (eV)	$\lambda$ (nm)	configuration
$S_0$	0.0	0	45.2% $(\sigma)^2(\pi)^4(\delta)^4$
			33.0% $(\sigma)^2(\pi)^4(\delta)^3(\delta^*)^1$
$T_1$	1.48	837	79.7% $(\sigma)^2(\pi)^4(\delta)^3(\delta^*)^1$
$T_2$	1.65	750	71.1% $(\sigma)^2(\pi)^4(\delta)^3(\delta^*)^1$
$T_3$	1.74	712	79.4% $(\sigma)^2(\pi)^4(\delta)^3(\delta^*)^1$
$S_2$	1.76	705	$80.6\%(\sigma)^2(\pi)^4(\delta)^3(\delta^*)^1$
$T_4$	1.82	682	75.9% $(\sigma)^2(\pi)^4(\delta)^3(\delta^*)^1$
$S_3$	1.84	673	79.4% $(\sigma)^2(\pi)^4(\delta)^3(\delta^*)^1$
$S_4$	1.98	626	79.6% $(\sigma)^2(\pi)^4(\delta)^3(\delta^*)^1$

used for uranium. All the other atoms (C and H) were treated using the def2-SVP basis set. All the DFT calculations were performed with the Gaussian 09 software.<sup>17</sup> Single-point calculations were performed at the PBE-D3 optimized geometries using the complete active space, CASSCF method, to gain insight into the electronic structure of the UTM-2 complexes. The ANO-RCC-vtzp basis set<sup>18</sup> was employed for U and TM, while a double-ζ quality ANO-RCC-vdzp basis set was used for N and P atoms. A minimal basis set of ANO-RCC type was used for C and H. Douglas-Kroll-Hess Hamiltonian was used to include scalar relativistic effects. 19 The active space employed in the CASSCF calculations consists of the valence 5f and 6d orbitals of U and the 3d and 4s orbitals of TM. Larger active-spaces were also explored; however, there were no changes in the final results (see Supporting Information (SI)). The electronic excitation energies were calculated at multistate complete active space second-order perturbation theory (MS-CASPT2) level of theory.<sup>20</sup> We used the default ionization-potential-electron-affinity (IPEA) shift of 0.25 au, which is an empirical correction applied to the zero-order Hamiltonian. We also applied an imaginary shift of 0.2 au to avoid possible intruder states. The Molcas 8.0 software package<sup>22</sup> was used for the CASSCF calculations.

The effective bond order (EBO) was calculated using the formula 1e

$$EBO = \frac{\sum_{i} (B_{i} - AB_{i})}{2}$$

where  $B_i$  and  $AB_i$  are the occupation numbers of bonding and antibonding natural orbital in an orbital pair, respectively, and the sum runs over all the orbital pairs.

## 3. RESULTS

Unrestricted DFT (UPBE-D3) calculations were performed for UTM-1 and UTM-2 (TM = Cr, Mn, Fe, Co, Ni) complexes for various possible spin states. Table 1 summarizes the results for different spin states for the UTM-1 complexes. The most stable spin state results are highlighted. DFT optimized geometries show that the shortest U-TM bond occurs between U and Mn atoms.

The most stable spin states for UCr-1, UMn-1, UFe-1, UCo-1, and UNi-1 complexes as determined from UPBE-D3 calculations are the doublet, singlet, doublet, triplet, and quartet state, respectively. The formal shortness ratio (FSR) is defined herein as the ratio of metal—metal bond distance to the sum of the metals' covalent radii. A FSR value of 1 suggests the presence of single bond, while a smaller value indicates multiple bonds. According to their FSR values, UCr-1, UMn-1, UFe-1, and UCo-1 complexes should have multiple bonds between the two metals, while the UNi-1 complex shows a weaker interaction.

The DFT results along with CASSCF and CASPT2 relative energies for UTM-2 are summarized in Table 2. The U-TM bond distance does not change significantly between UTM-1 and UTM-2. CASSCF and CASPT2 relative energies follow the same trend as DFT for all UTM-2 complexes with minor caveat for UCr-2. In UCr-2, CASSCF predicts a sextet ground spin state 0.4 kcal/mol lower in energy than the doublet; however, after application of the perturbative correction to the CASSCF energies (i.e., CASPT2), the doublet spin state appears as the ground state. The Mayer bond order for UTM-1 and UTM-2 at the ground spin state are reported in Table 3. For UCr and UMn complexes, the Mayer bond order is the same for the two ligands; however, UTM-2 favors shorter bond lengths for UFe, UCo, and UNi, which is in line with the trend seen in LuNi complexes with the two ligands. 12 To understand the nature of uranium and first-row transition metals, UTM-2 were further studied with multiconfigurational methods as they are smaller calculations and thus require fewer computational resources such as time and memory.

**3.1. UCr Complex.** In 2013, Infante and co-workers proposed a 6-fold bonding for a theoretical CrU diatomic molecule with an EBO of 5.3. However, this diatomic molecule could be experimentally synthesized only in extreme conditions. In this article, we investigate the nature of the bonding in synthetically motivated UCr[(iPr<sub>2</sub>PCH<sub>2</sub>NAr)<sub>3</sub>tacn] (UCr-1)

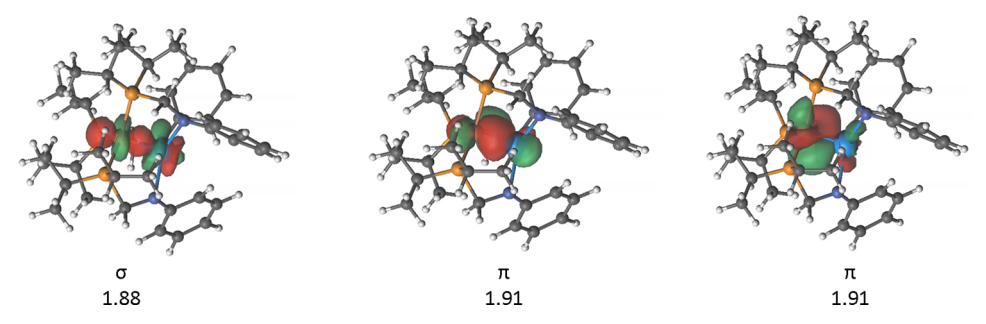


Figure 5. Bonding orbitals of UFe-2 complex along with the occupation number of the orbitals.

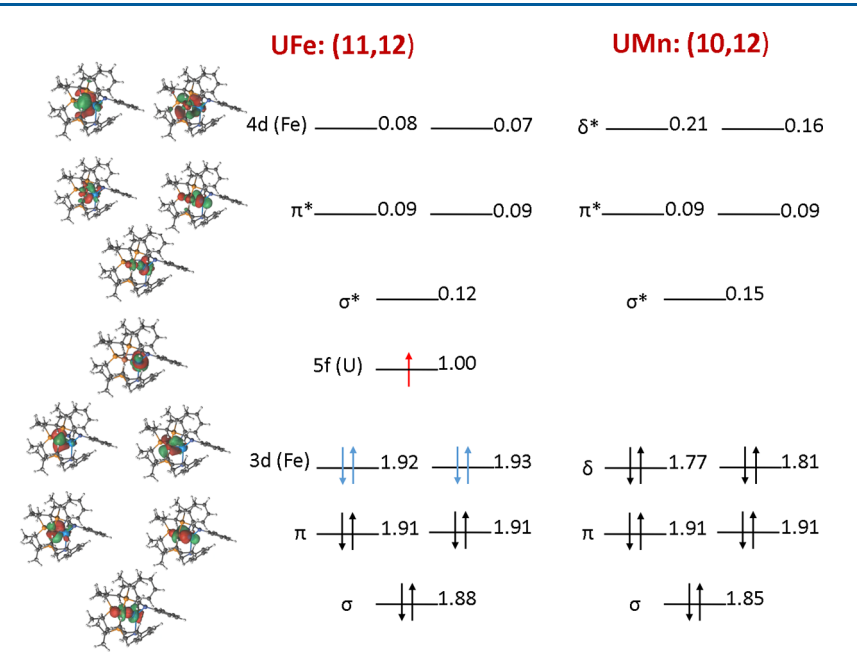


Figure 6. Comparison between the MO diagrams of UFe-2 and UMn-2 complexes. The blue and red colors represent electrons localized on Fe and U, respectively. The occupation numbers of the orbitals are listed above them.

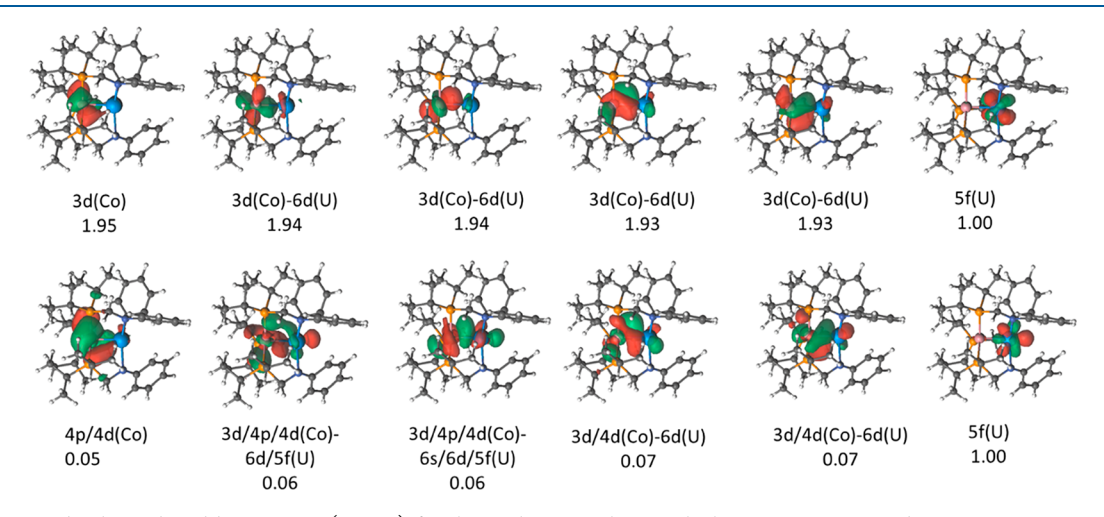
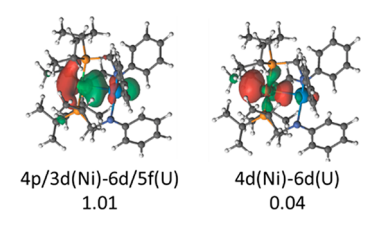


Figure 7. UCo-2 orbitals predicted by CASSCF(13, 12) for the triplet state along with their occupation numbers.

and  $UCr({}^{i}Pr_{2}PCH_{2}NAr)_{3}$  (UCr-2) complexes. Since the bond-distance between Cr and U and other geometric parameters are similar between the UCr-1 and UCr-2 complexes, we further investigated UCr-2 complex using multiconfigurational methods. Figure 2 shows a comparison between the previously reported electronic structure of the diatomic molecule CrU,  $^{8e}$  and the complex UCr-2 proposed in this study. The dominant electronic configuration of CrU is  $(1\sigma)^{2}(1\sigma)^{2}(1\pi)^{4}(1\delta)^{4}$ . The second  $\sigma$  bond in CrU has contributions from 7s and 6d of U. Since the U atom is formally  $U^{3+}$  in UCr-2 while it is  $U^{0}$  in CrU, we do not observe a second sigma  $(2\sigma)$  bond in UCr-2. The occupation numbers for CASSCF orbitals for UCr-2 are reported in Table 4. The EBO is calculated to be 3.3.

**3.2. UMn-2 Complex.** Inspection of the CASSCF wave function shows that UMn-2 is highly multiconfigurational, with a dominant configuration- $((\sigma)^2(\pi)^4(\delta)^4)$  with a weight of 70% and a second configuration- $((\sigma)^2(\pi)^4(\delta)^2(\delta^*)^2)$  with a weight of 7% and 7% weight for the configuration- $((\sigma)^2(\pi)^4(\delta)^2(\delta^*)^2)$ . A formal quintuple bond between



**Figure 8.** Bonding and antibonding orbitals in UNi-2 complexes along with their occupation numbers.

uranium and manganese with an EBO of 4.3 is predicted. Such a high bond order between uranium and manganese is unprecedented. Figure 3 shows the UMn-2 bonding and antibonding orbitals present in the active space. The atomic orbitals on Mn and U along with the resulting bonding orbitals are shown in Figure 4. The UMn-2  $\sigma$  and  $\delta$  bonding molecular orbitals contain minor contributions ( $\sim$ 5%) from uranium 6d atomic orbitals. The  $\sigma$ -type orbital contains major contributions from the U  $5f_z^3$  and the Mn  $3d_z^2$  orbitals, while the two  $\delta$ 

Table 6. Detailed DFT Natural Bond Orbital Analysis of UTM-2 Species

complex	orbital	%ТМ	%U	total electrons
UCr-2	$\sigma$ (alpha)	63.0 (3d: 84.4; 4p: 13.4)	37.0 (6d:7.8; 5f:90.2)	0.89
	$\pi$ (alpha)	65.3 (3d: 91.3; 4p: 8.7)	34.7 (5f:58.3;	0.89
	$\pi$ (alpha)	66.0	6d:40.3) 34.0	0.90
	(1)	(3d:82.4; 4p:17.6)	(6d:34.6; 5f:63.6)	
	$\delta$ (alpha)	63.8	36.23	0.88
		(3d: 79.6; 4p: 20.4)	(6d; 6.6; 5f: 92.8)	
	$\delta$ (alpha)	68.8	31.2	0.87
		(3d:85.4; 4p: 13.9)	(5f:90.0; 6d:9.4)	
	$\sigma$ (beta)	59.6	40.4	0.89
		(3d: 82.9; 4p: 15.1)	(6d:7.7; 5f:90.5)	
	$\pi$ (beta)	64.5	35.5	0.92
		(3d: 91.3; 4p: 8.7)	(5f:60.9; 6d:37.9)	
	$\pi$ (beta)	63.0	37.0	0.90
		(3d:81.3; 4p:18.6)	(6d:35.0; 5f:63.4)	
	$\delta$ (beta)	61.9	38.1	0.87
		(3d: 86.5; 4p: 12.9)	(6d; 8.0; 5f: 91.6)	
UMn-2	$\sigma$	66.6	33.4	1.77
		(3d: 87.8; 4p: 9.04)	(6d:8.9; 5f:89.9)	
	$\pi$	71.8	21.2	1.78
		(3d: 79.1; 4p: 20.9)	(6d; 67.7; 5f: 30.8)	
	$\pi$	70.5	29.5	1.74
		(3d:73.9; 4p: 26.1)	(5f:65.7; 6d:33.0)	
	δ	70.2	29.8	1.78
		(3d: 85.4; 4p: 14.6)	(5f:93.1; 6d:6.3)	
	δ	70.7	29.8	1.77
		(3d:85.8; 4p:14. CAS1_C2_1.52)	(6d:8.0; 5f:91.5)	
UFe-2	$\sigma$ (alpha)	73.6	26.4	0.90
		(3d: 89.2; 4p: 10.2)	(6d:16.2; 5f:82.6)	
	$\delta$ (alpha)	76.2	23.8	0.87
		(3d: 79.5; 4p: 16.3)	(6d; 16.8; 5f: 80.3)	
	$\delta$ (alpha)	80.4	19.6	0.92
		(3d: 97.5)	(6d:12.5; 5f: 86.3)	

orbitals are mainly composed of the U  $5f_{z(x^2-y^2)}$  and  $5f_{xyz}$  and Mn  $3d_{x^2-y^2}$  and  $3d_{xy}$ . The two  $\pi$ -orbitals also have major contributions from U 6d orbitals in addition to U  $5f_{yz}$ , Mn  $3d_{yz}$ , U  $5f_{xz}$  and Mn  $3d_{xz}$ .

To study the electronic spectra of UMn-2 complex, MS-CASPT2 was employed. The major configurations for all the low-lying excited states consist of  $\delta \rightarrow \delta^*$  transitions (Table 5). The MS-CASPT2 data show the first excited state to be a triplet state  $(T_1)$ .

The infrared-spectra were calculated at the UPBE-D3 level (SI). The U-Mn stretching is predicted at 474 cm<sup>-1</sup>, which

Table 7. Mulliken and LoProp Charges for U and TM in UTM-2 Complexes for the Most Stable Spin States

	τ	J	(	Cr
UCr-2(S = 2)	Mulliken	LoProp	Mulliken	LoProp
CASSCF	3.333	2.247	-0.476	-0.235
DFT	0.458	N/A	-0.276	N/A
	1	U	N	<b>I</b> n
UMn-2(S=0)	Mulliken	LoProp	Mulliken	LoProp
CASSCF	3.329	2.160	-0.692	-0.069
DFT	0.471	N/A	0.056	N/A
	τ	J	F	<sup>7</sup> e
UFe-2(S=2)	Mulliken	LoProp	Mulliken	LoProp
CASSCF	3.355	2.291	-0.516	-0.154
DFT	0.640	N/A	-0.161	N/A
	Ţ	J	(	Со
UCo-2(S = 3)	Mulliken	LoProp	Mulliken	LoProp
CASSCF	3.148	2.345	0.107	-0.171
DFT	0.799	N/A	-0.339	N/A
	τ	J	1	Ni .
UNi-2(S=4)	Mulliken	LoProp	Mulliken	LoProp
CASSCF	3.037	2.136	-0.259	-0.166
DFT	0.678	N/A	-0.206	N/A

is comparable to the IR-frequency reported for a nearly isostructural dichromium complex that is also quintuply bonded (434 cm<sup>-1</sup>);<sup>24</sup> P–Mn–P stretch are observed at 277 and 269 cm<sup>-1</sup>, respectively.

**3.3. UFe-2 Complex.** The UFe-2 complex shows a formal triple bond between U and Fe, with an effective bond order of 2.7. The three bonding orbitals are shown in Figure 5. A comparison of UFe-2 molecular orbital (MO) diagram shows that the Fe  $3d_z^2$ ,  $3d_{xz}$ , and  $3d_{yz}$  orbitals overlap with U  $5f_z^3$ ,  $5f_{xz}^2$ , and  $5f_{yz}^2$ . One would expect a higher bond order for UFe-2 based on the electronic configuration of Fe; however,  $3d_{x^2-y^2}$  and  $3d_{xy}$  are localized on the Fe center and, thus, do not participate in bonding. We compare the frontier molecular orbitals of UFe-2 and UMn-2 complexes in Figure 6. The unpaired electron of UFe-2 is localized on the uranium  $5f_{x(x^2-3y^2)}$  orbital.

3.4. UCo-2 and UNi-2 Complexes. The interaction between U and TM in UCo-2 is different from those in UMn-2 and UFe-2. Their bonding is more dative in nature, directed from the occupied Co 3d orbitals toward the U 6d orbitals while the U 5f orbitals do not participate in the bonding. Since the most stable spin state of the UCo-2 complex is the triplet state, the two unoccupied electrons are localized on U 5f orbitals. Although there are four orbitals with nonzero contributions from the uranium atom (Figure 7), only two orbitals show an effective overlap between U and Co where the contribution of uranium atom is more than 10% (Table 4). In contrast, in the UNi-2 complex with a quintet spin ground state, we observe the presence of half-a-bond (Figure 8) and a singly occupied orbital containing significant contributions from the U  $5f_{z^3}$  and Ni  $3d_{z^2}$  orbitals. Interestingly, the trends for bond order and bond length observed for UTM-2 are similar to observations made in the previously reported family of complexes  $TMCr(N(o-(NCH_2P^iPr_2)C_6H_4)_3)$  (TM = Mn, Fe, Co, Ni).1b

**3.5. Natural Bond Orbital Analysis.** The density functional natural bond orbital (NBO)<sup>25</sup> analysis studies

Table 8. Spin Densities for U and TM in UTM-2 Complexes for the Most Stable Spin States

U	UCr-2		in-2	U	Fe-2	UCo-2		UNi-2	
U	Cr	U	Mn	U	Fe	U	Со	U	Ni
0.266	0.620	0.000	0.000	1.368	-0.337	2.226	-0.157	3.003	-0.060

**Figure 9.** Schematic representation of (left) [(<sup>i</sup>Pr<sub>2</sub>PCH<sub>2</sub>NAr)<sub>3</sub>tacn]U (LU-1) and (right) (<sup>i</sup>Pr<sub>2</sub>PCH<sub>2</sub>NPh)<sub>3</sub>U (LU-2).

Table 9. Binding Energies (kcal/mol) for UTM-1 and UTM-2<sup>a</sup>

	UCr	UMn	UFe	UCo	UNi
UTM-1	-84.7	-111.6	-136.5	-135.6	-123.9
UTM-2	-78.5	-105.4	-130.2	-129.5	-116.2
$^{a}LU = [(^{i}P)$	h <sub>2</sub> PCH <sub>2</sub> N)	$C_6H_5]_3U$ .			

predict quadruple bonds in UCr-2 and 5-fold bonding in UMn-2 (Table 6). In case of UCr-2, DFT NBO calculation also predicts the presence of a half delta bond in addition to the four bonding MOs predicted by CASSCF studies. For the UMn-2 complex, CASSCF and NBO agree well where both methods predict the presence of a quintuple bond between U and Mn. Strangely, for the UFe-2 molecule, only alpha spin orbitals show the presence of molecular bonds between U and Fe, while no bonding MOs are found among beta spin orbitals. It should be noted that these bimetallic complexes are highly multireference and DFT NBO calculations are not always reliable.

**3.6.** Charge and Spin Density Analysis. The Mulliken<sup>26</sup> and LoProp<sup>27</sup> charge densities are shown in Table 7. While the CASSCF LoProp charge density on U remains almost constant along the series, for TM, it increases from Cr to Mn and then decreases again for Fe and does not change significantly thereafter. DFT and CASSCF Mulliken charge densities present different trends for U and TM. The spin densities obtained from unrestricted DFT calculations show that the unpaired electron is located on Cr in UCr-2, while it is located on U rather than on TM in UFe-2, UCo-2, and UNi-2 (Table 8). These results are in agreement with the picture that emerges from the CASSCF MOs analysis (Figures 2, 6, and 7).

**3.7. Binding Energies.** We also calculated the binding energies by subdividing UTM-1 and UTM-2 into the following fragments: UTM-1 is divided up into [(iPr<sub>2</sub>PCH<sub>2</sub>NAr)<sub>3</sub>tacn]U (which we name LU-1) and TM, and UTM-2 is divided up into (iPr<sub>2</sub>PCH<sub>2</sub>NPh)<sub>3</sub>U (which we name LU-2) and TM (Figure 9). The binding energies were calculated at the DFT level for the most stable spin state of each species (Table 9). The optimized LU-1 and LU-2 species have a quartet ground state. The binding energies do not follow the same trend as the bond-orders since these are not diatomic molecules and the ligand also plays a role. The binding energies increase from UCr-1 to UFe-1 then decrease from UFe-1 to UNi-1; a similar trend is observed for the UTM-2 complexes. Although, the U-TM bond lengths are shorter in UTM-2 than in UTM-1, the binding energies are higher for UTM-1 suggesting that TM is

bound more strongly to the phosphine ligands in UTM-1 than in UTM-2.

#### 4. CONCLUSIONS

In summary, we presented a study of the bonding of uranium with the first-row transition metals Cr, Mn, Fe, Co, and Ni, in the UTM[(iPr<sub>2</sub>PCH<sub>2</sub>NAr)<sub>3</sub>tacn] (UTM-1) and UTM-(Pr<sub>2</sub>PCH<sub>2</sub>NAr)<sub>3</sub> (UTM-2) species. Higher bond orders have yet to be obtained (or predicted) between a transition metal and uranium, and our predictions point to which specific metal-metal pairing will ultimately lead to these higher order TM-U bonds. A systematic study of the uranium-first-row transition metal interaction demonstrates the wide tunability of bond orders across the period, ranging from formally quintuple to single by replacing the transition metal in UTM-2. The periodic trend shows an increase in bond order from Cr to Mn and then a decrease across the period. We predict for the first time 5-fold bonding between U and Mn in the synthetically inspired complexes: UMn-2. The electronic spectra of UMn-2 complex shows low-lying  $\delta \to \delta^*$  singlet and triplet transitions. We observed the presence of dative bonds in UCo-2, which are directed from the 3d orbitals of Co to the unoccupied 6d orbital of uranium, while UNi contains a half bond between U and Ni. Our study will help the future design of novel uranium-transition metal compounds with multiple bonds.

#### ASSOCIATED CONTENT

# S Supporting Information

The Supporting Information is available free of charge on the ACS Publications website at DOI: 10.1021/acs.inorgchem.9b01264.

Orbitals and active spaces, partial atomic charges and spin populations, structures, computed infrared spectra, binding energies, CASSCF and MS-CASPT2 absolute energies (PDF)

CASSCF optimized natural orbitals in the Molcas format (RasOrb, plain text) (ZIP)

# AUTHOR INFORMATION

## **Corresponding Author**

\*E-mail: gagliard@umn.edu.

ORCID

Prachi Sharma: 0000-0002-1819-542X Bianca L. Ramirez: 0000-0001-7907-6312 Connie C. Lu: 0000-0002-5162-9250 Laura Gagliardi: 0000-0001-5227-1396

**Notes** 

The authors declare no competing financial interest.

## ACKNOWLEDGMENTS

We thank Stephen T. Liddle, Shu-Xian Hu, and Weston Shelander for helpful discussions. This work was supported by the Division of Chemical Sciences, Geosciences, and Biosciences, Office of Basic Energy Sciences, of the U.S. Department of Energy under Grant USDOE/DESC002183. B.L.R. is supported by the American Chemical Society Petroleum

Research Fund (57192-ND3), and C.C.L. acknowledges the National Science Foundation (CHE-1665010).

#### REFERENCES

(1) (a) Frenking, G. Building a quintuple bond. Science 2005, 310 (5749), 796-797. (b) Clouston, L. J.; Siedschlag, R. B.; Rudd, P. A.; Planas, N.; Hu, S.; Miller, A. D.; Gagliardi, L.; Lu, C. C. Systematic Variation of Metal-Metal Bond Order in Metal-Chromium Complexes. J. Am. Chem. Soc. 2013, 135 (35), 13142-13148. (c) Rudd, P. A.; Liu, S.; Planas, N.; Bill, E.; Gagliardi, L.; Lu, C. C. Multiple Metal-Metal Bonds in Iron-Chromium Complexes. Angew. Chem. 2013, 125 (16), 4545-4548. (d) Noor, A.; Wagner, F. R.; Kempe, R. Metal-metal distances at the limit: A coordination compound with an ultrashort chromium-chromium bond. Angew. Chem., Int. Ed. 2008, 47 (38), 7246-7249. (e) Roos, B. O.; Borin, A. C.; Gagliardi, L. Reaching the maximum multiplicity of the covalent chemical bond. Angew. Chem., Int. Ed. 2007, 46 (9), 1469-1472. (f) Cotton, F.; Curtis, N.; Harris, C.; Johnson, B.; Lippard, S.; Mague, J.; Robinson, W.; Wood, J. Mononuclear and polynuclear chemistry of rhenium (III): its pronounced homophilicity. Science 1964, 145 (3638), 1305-1307. (g) Cotton, F.; Curtis, N.; Johnson, B.; Robinson, W. Compounds containing dirheniurm (III) octahalide anions. Inorg. Chem. 1965, 4 (3), 326-330. (h) Cotton, F. Multiple metal-metal bonds. J. Chem. Educ. 1983, 60 (9), 713. (i) Nguyen, T.; Sutton, A. D.; Brynda, M.; Fettinger, J. C.; Long, G. J.; Power, P. P. Synthesis of a stable compound with fivefold bonding between two chromium (I) centers. Science 2005, 310 (5749), 844-847. (j) Cotton, F. A.; Murillo, C. A.; Walton, R. A. Multiple Bonds between Metal Atoms; Springer Science & Business Media, 2005. (k) Tsai, Y. C.; Hsu, C. W.; Yu, J. S. K.; Lee, G. H.; Wang, Y.; Kuo, T. S. Remarkably Short Metal-Metal Bonds: A Lantern-Type Quintuply Bonded Dichromium (I) Complex. Angew. Chem., Int. Ed. 2008, 47 (38), 7250-7253. (1) Hsu, C. W.; Yu, J. S. K.; Yen, C. H.; Lee, G. H.; Wang, Y.; Tsai, Y. C. Quintuply-Bonded Dichromium (I) Complexes Featuring Metal-Metal Bond Lengths of 1.74 Å. Angew. Chem. 2008, 120 (51), 10081-10084. (m) Greenwood, B. P.; Rowe, G. T.; Chen, C.-H.; Foxman, B. M.; Thomas, C. M. Metal- Metal Multiple Bonds in Early/Late Heterobimetallics Support Unusual Trigonal Monopyramidal Geometries at both Zr and Co. J. Am. Chem. Soc. 2010, 132 (1), 44-45. (n) Collman, J. P.; Boulatov, R. Heterodinuclear Transition-Metal Complexes with Multiple Metal-Metal Bonds. Angew. Chem., Int. Ed. 2002, 41 (21), 3948-3961. (o) Powers, I. G.; Uyeda, C. Metal-metal bonds in catalysis. ACS Catal. 2017, 7 (2), 936-958.

(2) (a) Oelkers, B.; Kempe, R. Group 3, Lanthanide, and Actinide Metal-Metal Bonds. Molecular Metal-Metal Bonds: Compounds, Synthesis, Properties 2015, 47-71. (b) Butovskii, M. V.; Kempe, R. Rare earth-metal bonding in molecular compounds: recent advances, challenges, and perspectives. New J. Chem. 2015, 39 (10), 7544-7558. (c) Oelkers, B.; Butovskii, M. V.; Kempe, R. f-Element-Metal Bonding and the Use of the Bond Polarity To Build Molecular Intermetalloids. Chem. - Eur. J. 2012, 18 (43), 13566-13579. (d) Hrobárik, P.; Straka, M.; Pyykkö, P. Computational study of bonding trends in the metalloactinyl series EThM and MThM'(E= N-, O, F+; M, M'= Ir-, Pt, Au+). Chem. Phys. Lett. 2006, 431 (1-3), 6-12. (e) Santos, M.; Marcalo, J.; Pires de Matos, A.; Gibson, J. K.; Haire, R. G. Actinide-Transition Metal Heteronuclear Ions and Their Oxides:{IrUO}+ as an Analogue to Uranyl. Eur. J. Inorg. Chem. 2006, 2006 (17), 3346-3349. (f) Gagliardi, L.; Pyykkö, P. Theoretical Search for Very Short Metal-Actinide Bonds: NUIr and Isoelectronic Systems. Angew. Chem., Int. Ed. 2004, 43 (12), 1573-1576.

- (3) Bennett, R.; Bruce, M.; Stone, F. Tetrakis (pentacarbonylmanganese) uranium. *J. Organomet. Chem.* **1971**, *26* (3), 355–356.
- (4) Sternal, R. S.; Marks, T. J. Actinide-to-transition metal bonds. Synthesis, characterization, and properties of metal-metal bonded systems having the tris (cyclopentadienyl) actinide fragment. *Organometallics* **1987**, *6* (12), 2621–2623.
- (S) Bucaille, A.; Le Borgne, T.; Ephritikhine, M.; Daran, J.-C. Synthesis and X-ray Crystal Structure of a Urana [1] ferrocenophane,

the First Tris'(1, 1 -ferrocenylene) Metal Compound. *Organometallics* **2000**, 19 (23), 4912–4914.

(6) Cordero, B.; Gómez, V.; Platero-Prats, A. E.; Revés, M.; Echeverría, J.; Cremades, E.; Barragán, F.; Alvarez, S. Covalent radii revisited. *Dalton Transactions* **2008**, No. 21, 2832–2838.

(7) (a) Gardner, B. M.; McMaster, J.; Moro, F.; Lewis, W.; Blake, A. J.; Liddle, S. T. An unsupported uranium-rhenium complex prepared by alkane elimination. Chem. - Eur. J. 2011, 17 (25), 6909-6912. (b) Patel, D.; King, D. M.; Gardner, B. M.; McMaster, J.; Lewis, W.; Blake, A. J.; Liddle, S. T. Structural and theoretical insights into the perturbation of uranium-rhenium bonds by dative Lewis base ancillary ligands. Chem. Commun. 2011, 47 (1), 295-297. (c) Gardner, B. M.; McMaster, J.; Lewis, W.; Liddle, S. T. Synthesis and structure of [{N (CH 2 CH 2 NSiMe 3) 3} URe ( $\eta$  5-C 5 H 5) 2]: a heterobimetallic complex with an unsupported uraniumrhenium bond. Chem. Commun. 2009, No. 20, 2851-2853. (d) Gardner, B. M.; Patel, D.; Cornish, A. D.; McMaster, J.; Lewis, W.; Blake, A. J.; Liddle, S. T. The nature of unsupported uraniumruthenium bonds: a combined experimental and theoretical study. Chem. - Eur. J. 2011, 17 (40), 11266-11273. (e) Monreal, M. J.; Diaconescu, P. L. A weak interaction between iron and uranium in uranium alkyl complexes supported by ferrocene diamide ligands. Organometallics 2008, 27 (8), 1702-1706. (f) Monreal, M. J.; Carver, C. T.; Diaconescu, P. L. Redox Processes in a Uranium Bis (1, 1 '-diamidoferrocene) Complex. Inorg. Chem. 2007, 46 (18), 7226-7228. (g) Diaconescu, P. L.; Odom, A. L.; Agapie, T.; Cummins, C. C. Uranium- Group 14 Element Single Bonds: Isolation and Characterization of a Uranium (IV) Silyl Species. Organometallics 2001, 20 (24), 4993-4995. (h) Napoline, J. W.; Kraft, S. J.; Matson, E. M.; Fanwick, P. E.; Bart, S. C.; Thomas, C. M. Tris-(phosphinoamide)-Supported Uranium-Cobalt Heterobimetallic Complexes Featuring Co → U Dative Interactions. *Inorg. Chem.* 2013, 52 (20), 12170-12177. (i) Ward, A. L.; Lukens, W. W.; Lu, C. C.; Arnold, J. Photochemical route to actinide-transition metal bonds: synthesis, characterization and reactivity of a series of thorium and uranium heterobimetallic complexes. J. Am. Chem. Soc. 2014, 136 (9), 3647-3654. (j) Hlina, J. A.; Pankhurst, J. R.; Kaltsoyannis, N.; Arnold, P. L. Metal-Metal Bonding in Uranium-Group 10 Complexes. J. Am. Chem. Soc. 2016, 138 (10), 3333-3345. (k) Chi, C.; Wang, J. Q.; Qu, H.; Li, W. L.; Meng, L.; Luo, M.; Li, J.; Zhou, M. Preparation and Characterization of Uranium-Iron Triple-Bonded UFe (CO) 3- and OUFe (CO) 3- Complexes. Angew. Chem. 2017, 129 (24), 7036-7040. (1) Feng, G.; Zhang, M.; Shao, D.; Wang, X.; Wang, S.; Maron, L.; Zhu, C. Transition-metal-bridged bimetallic clusters with multiple uranium-metal bonds. Nat. Chem. 2019, 11, 248. (m) Patel, D.; Moro, F.; McMaster, J.; Lewis, W.; Blake, A. J.; Liddle, S. T. A Formal High Oxidation State Inverse-Sandwich Diuranium Complex: A New Route to f-Block-Metal Bonds. Angew. Chem. 2011, 123 (44), 10572-10576. (n) Lu, E.; Wooles, A. J.; Gregson, M.; Cobb, P. J.; Liddle, S. T. A very short uranium (iv)rhodium (i) bond with net double-dative bonding character. Angew. Chem. 2018, 130 (22), 6697-6701. (o) Ayres, A. J.; Zegke, M.; Ostrowski, J. P.; Tuna, F.; McInnes, E. J.; Wooles, A. J.; Liddle, S. T. Actinide-transition metal bonding in heterobimetallic uranium-and thorium-molybdenum paddlewheel complexes. Chem. Commun. **2018**, *54* (96), 13515–13518.

(8) (a) Vlaisavljevich, B.; Miró, P.; Cramer, C. J.; Gagliardi, L.; Infante, I.; Liddle, S. T. On the Nature of Actinide—and Lanthanide—Metal Bonds in Heterobimetallic Compounds. *Chem. - Eur. J.* 2011, 17 (30), 8424–8433. (b) Bi, Y.-T.; Li, L.; Guo, Y.-R.; Pan, Q.-J. Heterobimetallic Uranium—Nickel/Palladium/Platinum Complexes of Phosphinoaryl Oxide Ligands: A Theoretical Probe for Metal—Metal Bonding and Electronic Spectroscopy. *Inorg. Chem.* 2019, 58, 1290. (c) Chi, X.-W.; Wu, Q.-Y.; Hao, Q.; Lan, J.-H.; Wang, C.-Z.; Zhang, Q.; Chai, Z.-F.; Shi, W.-Q. Theoretical Study on Unsupported Uranium—Metal Bonding in Uranium—Group 8 Complexes. *Organometallics* 2018, 37 (21), 3678–3686. (d) Fortier, S.; Aguilar-Calderón, J. R.; Vlaisavljevich, B.; Metta-Magaña, A. J.; Goos, A. G.; Botez, C. E. An N-Tethered Uranium (III) Arene Complex and the Synthesis of

an Unsupported U-Fe Bond. Organometallics 2017, 36 (23), 4591–4599. (e) Ruiperez, F.; Merino, G.; Ugalde, J. M.; Infante, I. Molecules with high bond orders and ultrashort bond lengths: CrU, MoU, and WU. Inorg. Chem. 2013, 52 (6), 2838–2843.

- (9) Roos, B. O.; Taylor, P. R.; Siegbahn, P. E. A complete active space SCF method (CASSCF) using a density matrix formulated super-CI approach. *Chem. Phys.* **1980**, *48* (2), 157–173.
- (10) (a) Gagliardi, L.; Willetts, A.; Skylaris, C.-K.; Handy, N. C.; Spencer, S.; Ioannou, A. G.; Simper, A. M. A relativistic density functional study on the uranium hexafluoride and plutonium hexafluoride monomer and dimer species. J. Am. Chem. Soc. 1998, 120 (45), 11727-11731. (b) Gagliardi, L.; Grenthe, I.; Roos, B. O. A theoretical study of the structure of tricarbonatodioxouranate. Inorg. Chem. 2001, 40 (13), 2976-2978. (c) Gagliardi, L.; Pyykkö, P.; Roos, B. O. A very short uranium-uranium bond: The predicted metastable U 2 2+. Phys. Chem. Chem. Phys. 2005, 7 (12), 2415-2417. (d) Gagliardi, L.; Roos, B. O. Quantum chemical calculations show that the uranium molecule U 2 has a quintuple bond. Nature 2005, 433 (7028), 848. (e) Roos, B. O.; Malmqvist, P.-Å.; Gagliardi, L. Exploring the Actinide- Actinide Bond: Theoretical Studies of the Chemical Bond in Ac2, Th2, Pa2, and U2. J. Am. Chem. Soc. 2006, 128 (51), 17000-17006. (f) Knecht, S.; Jensen, H. J. A.; Saue, T. Relativistic quantum chemical calculations show that the uranium molecule U 2 has a quadruple bond. Nat. Chem. 2019, 11 (1), 40.
- (11) (a) King, D. M.; Tuna, F.; McInnes, E. J.; McMaster, J.; Lewis, W.; Blake, A. J.; Liddle, S. T. Synthesis and structure of a terminal uranium nitride complex. *Science* **2012**, 337 (6095), 717–720. (b) Mills, D. P.; Cooper, O. J.; Tuna, F.; McInnes, E. J.; Davies, E. S.; McMaster, J.; Moro, F.; Lewis, W.; Blake, A. J.; Liddle, S. T. Synthesis of a Uranium (VI)-Carbene: Reductive Formation of Uranyl (V)-Methanides, Oxidative Preparation of a [R<sub>2</sub>C=U=O]<sup>2+</sup> Analogue of the [O=U=O]<sup>2+</sup> Uranyl Ion (R= Ph<sub>2</sub>PNSiMe<sub>3</sub>), and Comparison of the Nature of U<sup>IV</sup>=C, U<sup>V</sup>= C, and U<sup>VI</sup>=C Double Bonds. *J. Am. Chem. Soc.* **2012**, 134 (24), 10047–10054. (c) Brown, J. L.; Fortier, S.; Lewis, R. A.; Wu, G.; Hayton, T. W. A Complete Family of Terminal Uranium Chalcogenides, [U (E)(N {SiMe3} 2) 3]–(E= O, S, Se, Te). *J. Am. Chem. Soc.* **2012**, 134 (37), 15468–15475.
- (12) Ramirez, B. L.; Sharma, P.; Eisenhart, R. J.; Gagliardi, L.; Lu, C. Bimetallic Nickel-Lutetium complexes: Tuning the properties and catalytic hydrogenation activity of the Ni site by varying the Lu coordination environment. *Chemical Science* **2019**, *10*, 3375.
- (13) Perdew, J. P.; Burke, K.; Ernzerhof, M. Generalized gradient approximation made simple. *Phys. Rev. Lett.* **1996**, 77 (18), 3865.
- (14) Grimme, S.; Antony, J.; Ehrlich, S.; Krieg, H. A consistent and accurate ab initio parametrization of density functional dispersion correction (DFT-D) for the 94 elements H-Pu. *J. Chem. Phys.* **2010**, 132 (15), 154104.
- (15) Weigend, F.; Ahlrichs, R. Balanced basis sets of split valence, triple zeta valence and quadruple zeta valence quality for H to Rn: Design and assessment of accuracy. *Phys. Chem. Chem. Phys.* **2005**, 7 (18), 3297–3305.
- (16) Martin, J. M.; Sundermann, A. Correlation consistent valence basis sets for use with the Stuttgart–Dresden–Bonn relativistic effective core potentials: The atoms Ga–Kr and In–Xe. *J. Chem. Phys.* **2001**, *114* (8), 3408–3420.
- (17) Frisch, M. J.; Trucks, G. W.; Schlegel, H. B.; Scuseria, G. E.; Robb, M. A.; Cheeseman, J. R.; Scalmani, G.; Barone, V.; Mennucci, B.; Petersson, G. A.; Nakatsuji, H.; Caricato, M.; Li, X.; Hratchian, H. P.; Izmaylov, A. F.; Bloino, J.; Zheng, G.; Sonnenberg, J. L.; Hada, M.; Ehara, M.; Toyota, K.; Fukuda, R.; Hasegawa, J.; Ishida, M.; Nakajima, T.; Honda, Y.; Kitao, O.; Nakai, H.; Vreven, T.; Montgomery, J. A., Jr.; Peralta, J. E.; Ogliaro, F.; Bearpark, M.; Heyd, J. J.; Brothers, E.; Kudin, K. N.; Staroverov, V. N.; Kobayashi, R.; Normand, J.; Raghavachari, K.; Rendell, A.; Burant, J. C.; Iyengar, S. S.; Tomasi, J.; Cossi, M.; Rega, N.; Millam, J. M.; Klene, M.; Knox, J. E.; Cross, J. B.; Bakken, V.; Adamo, C.; Jaramillo, J.; Gomperts, R.; Stratmann, R. E.; Yazyev, O.; Austin, A. J.; Cammi, R.; Pomelli, C.; Ochterski, J. W.; Martin, R. L.; Morokuma, K.; Zakrzewski, V. G.;

Voth, G. A.; Salvador, P.; Dannenberg, J. J.; Dapprich, S.; Daniels, A. D.; Farkas, O.; Foresman, J. B.; Ortiz, J. V.; Cioslowski, J.; Fox, D. J. *Gaussian 09*, revision A.02; Gaussian, Inc.: Wallingford, CT, 2009.

- (18) Roos, B. O.; Lindh, R.; Malmqvist, P.-Å.; Veryazov, V.; Widmark, P.-O. Main group atoms and dimers studied with a new relativistic ANO basis set. *J. Phys. Chem. A* **2004**, *108* (15), 2851–2858.
- (19) (a) Douglas, M.; Kroll, N. M. Quantum electrodynamical corrections to the fine structure of helium. *Ann. Phys.* **1974**, 82 (1), 89–155. (b) Hess, B. A. Relativistic electronic-structure calculations employing a two-component no-pair formalism with external-field projection operators. *Phys. Rev. A: At., Mol., Opt. Phys.* **1986**, 33 (6), 3742.
- (20) (a) Andersson, K.; Malmqvist, P. A.; Roos, B. O.; Sadlej, A. J.; Wolinski, K. Second-order perturbation theory with a CASSCF reference function. *J. Phys. Chem.* **1990**, 94 (14), 5483–5488. (b) Finley, J.; Malmqvist, P.-Å.; Roos, B. O.; Serrano-Andrés, L. The multi-state CASPT2 method. *Chem. Phys. Lett.* **1998**, 288 (2–4), 299–306.
- (21) Ghigo, G.; Roos, B. O.; Malmqvist, P.-Å. A modified definition of the zeroth-order Hamiltonian in multiconfigurational perturbation theory (CASPT2). *Chem. Phys. Lett.* **2004**, 396 (1–3), 142–149.
- (22) Aquilante, F.; Autschbach, J.; Carlson, R. K.; Chibotaru, L. F.; Delcey, M. G.; De Vico, L.; Fdez. Galván, I.; Ferré, N.; Frutos, L. M.; Gagliardi, L.; et al. Molcas 8: New capabilities for multiconfigurational quantum chemical calculations across the periodic table. *J. Comput. Chem.* **2016**, *37* (5), 506–541.
- (23) (a) Pyykkö, P. Additive covalent radii for single-, double-, and triple-bonded molecules and tetrahedrally bonded crystals: a summary. *J. Phys. Chem. A* **2015**, *119* (11), 2326–2337. (b) Cotton, F. A. Discovering and understanding multiple metal-to-metal bonds. *Acc. Chem. Res.* **1978**, *11* (6), 225–232. (c) Pyykkö, P.; Atsumi, M. Molecular single-bond covalent radii for elements 1–118. *Chem. Eur. J.* **2009**, *15* (1), 186–197.
- (24) Eisenhart, R. J.; Rudd, P. A.; Planas, N.; Boyce, D. W.; Carlson, R. K.; Tolman, W. B.; Bill, E.; Gagliardi, L.; Lu, C. C. Pushing the Limits of Delta Bonding in Metal—Chromium Complexes with Redox Changes and Metal Swapping. *Inorg. Chem.* **2015**, *54* (15), 7579—7592.
- (25) (a) Zimmerman, H. E., VIII. Development of Theory with Computation. *Computational Photochemistry* **2005**, *16*, 255. (b) Glendening, E. D.; Reed, A. E.; Carpenter, J. E.; Weinhold, F. *NBO Version 3.1* 1988.
- (26) Mulliken, R. S. Electronic population analysis on LCAO -MO molecular wave functions. I. *J. Chem. Phys.* **1955**, 23 (10), 1833–1840.
- (27) Gagliardi, L.; Lindh, R.; Karlström, G. Local properties of quantum chemical systems: The LoProp approach. *J. Chem. Phys.* **2004**, *121* (10), 4494–4500.